私立東海大學

資訊工程與科學研究所

碩士論文

指導教授：黃育仁 博士

可調式影像自動偵測技術於間接性螢光顯影分析

Adaptive Automatic Segmentation and Classification of HEp-2 Cells in Indirect Immunofluorescence Images

研究生：饒育郎

中 華 民 國 九 十 七 年 六 月

摘要

在組織性自我免疫的疾病中，HEp-2 細胞的間接性螢光切片檢查，廣泛地被用於檢測抗核抗體(antinuclear autoantibody, ANA)的存在性。抗核抗體主要的用途是能夠掃描出大範圍的抗體存在與否，而且 ANA 的類型是可以用螢光性的樣本清楚地描述出來。這些螢光性的樣本，必須經常由醫師在親自觀察切片的同時，藉由顯微鏡的幫助下，才能有客觀及詳盡的定義。然而，就是因為缺乏自動化的檢驗流程及標準化的作業程序，才會讓這樣的檢驗過程，仍然需要在專業且具有相當經驗的醫師或技術人員的指導下，才能獲得精確的診斷結果。因此在這樣的環境下，本論文提出了可以在間接性螢光切片的影像中，自動化檢測出螢光性樣本的系統，希望能用來協助醫師，即使在沒有專業技師協助操作之下，也能有相當正確的評斷結果。由於近幾年 ANA 的使用愈來愈普及的情況下，這樣的一個功能完善且自動化的檢驗系統，是不可或缺的，在臨床醫學的應用上，相信此系統的需求性，將會與日劇增。

刪除: 審查

刪除: 可

刪除: 在這樣的環境下，

刪除: 幫助

刪除: 具備

刪除: 知識的

刪除: 必然

刪除: 。此外

關鍵字：組織性自我免疫、影像切割、間接性螢光切片檢查、抗核抗體。

ABSTRACT

Indirect immunofluorescence (IIF) with HEp-2 cells is used for the detection of antinuclear autoantibodies (ANA) in systemic autoimmune diseases. The ANA testing allows to scan a broad range of autoantibody entities and to describe them by distinct fluorescence patterns. The fluorescence patterns are usually identified by physician manual inspecting the slides with the help of a microscope. However, due to lacking in satisfied automation of inspection and a low level of standardization, this procedure still needs highly specialized and experienced technician or physician to obtain diagnostic result. For this purpose, automatic inspection for fluorescence patterns in IIF image may assist physicians, without relevant experience, in making correct diagnosis. As ANA testing becomes more widespread used, a functional automatic inspection system is essential and its clinical application is becoming urgent.

Keywords: antinuclear autoantibodies, image segmentation, immunofluorescence pattern

INDEX

删除: 15

LIST OF TABLES

刪除: 32

LIST OF FIGURES

刪除: 12

刪除: 13

刪除: 14

刪除: 17

刪除: 20

删除: 21

删除: 30

CHAPTER 1

INTRODUCTION

Most of image segmentation techniques can be categorized as semiautomatic and automatic. Semiautomatic approaches usually provide reliable segmentation results but require the participation of a user in the image segmentation process [1]. Automatic image segmentation methods are usually nonparametric and generally based on local image information such as regions, edges, histograms, or clusters. In the past years, many methods for the segmentation of cell images have been presented [2-7]. These methods include region-based methods [8-10], edge-based methods [11-13], histogram-based methods [14], etc. The studies use the gray information of an image mainly without using any priori knowledge of a specific type of image. For some simple images with slight noise, these methods may work well. However, when an image contains extensive noise, clutter, or occlusion, it is difficult to obtain good segmentation results with these methods. Thus the segmentation performance has greatly improved by incorporating some a priori knowledge about the specific type of images being processed.

In general, pathologists might make diagnostic decision by observing the specimen cells and the geometric parameters of the cell such as the area, radius and the circumference. The information is very useful using computer-aided system to

删除: They

删除: without or

删除: low

删除: But

删除: in the presence of

删除: and

删除: However, t

删除: It

accurately measure the geometric parameters of the cell. Accurate segmentation of cell images is required to get the parameters. Because of the identification of the patterns has up to now been done manually by a human inspecting the slides with the help of a microscope. The lacking automation of this technique has resulted in the development of alternative techniques based on chemical reactions, which have not the discrimination power of the ANA testing. An automatic system would pave the way for a wider use of ANA testing.

An automatic inspection system for ANA testing can be divided into HEp-2 cell detection, fluorescence pattern classification and computer aided diagnosis phases. This study presented an efficient method for automatically detecting cells with fluorescence pattern in IIF images. The preprocessing of the proposed method reduces the any amount of noises but preserves the shape and contrast of cells. Then an adaptive edged-based segmentation automatically extracts outlines of cells in IIF images. The proposed method evaluated 2573 cells with six distinct fluorescence patterns from 45 images. The results of computer simulations revealed that the proposed method always identified cell outlines as were obtained by manual sketched. Such a method provides robust and fast automatic segmentation of HEp-2 fluorescent patterns in ANA testing. The proposed automatic segmentation system can save much of the time required to locate fluorescence patterns with very high stability.

刪除: To get the parameters, a

刪除: We

The rest of this paper is organized as follows. Chapter 2 presents the proposed methods. Chapter 3 discuss the texture features analysis for the IIF images. Chapter 4 shows the experiment results and evaluation, and the conclusion follows in chapter 5.

删除: our

删除: is

CHAPTER 2

MATERIALS AND METHODS

2.1 DATA ACQUISITION

This study used slides of HEp-2 substrate, at a serum dilution of 1:80. A physician takes images of slides with an acquisition unit consisting of the fluorescence microscope coupled with a commonly used fluorescence microscope (Axioskop 2, CarlZeiss, Jena, Germany) at 40-fold magnification. The immunofluorescence images were taken by an operator with a color digital camera (E-330, Olympus, Tokyo, Japan). The digitized images were of 8-bit photometric resolution for each RGB (Red, Green and Blue) color channel with a resolution of 3136×2352 pixel. Finally, the images were transferred to a personal computer and stored as *.orf-files (Raw data format) without compression. The image database containing 45 samples were collected from January 2007 to July 2007. Due to the size of original images was too large to adapt a segmentation procedure, thus this study down-sampled the image to a reasonable resolution 1024×768 pixel.

2.2 AUTOANTIBODY FLUORESCENCE PATTERNS

To evaluate the proposed system, this study included six different main patterns:

1. Diffuse pattern
2. Peripheral pattern
3. Coarse speckled pattern
4. Fine speckled pattern
5. Discrete speckled pattern
6. Nucleolar pattern

Figures 1 illustrate the distinct autoantibody fluorescence patterns. In the view point of image processing, the fluorescence cell belongs to diffuse, peripheral, coarse speckled, or fine speckled pattern normally includes only one connected region. On the contrary, the discrete speckled and nucleolar patterns consist of mass and several connected regions, respectively.

2.3 SIMPLE CLASSIFICATION PROCEDURE

Several studies have been proposed to classify autoantibody fluorescence patterns by using an automatic thresholding method, i.e. the Otsu's algorithm [15], to segment the cells. The thresholding method can choose the threshold to minimize the intra-class variance of the black and white pixels automatically. Due to the variety of ANA patterns, the Otsu's algorithm always failed to segment cells of discrete speckled and nucleolar patterns directly. Figure 2 shows the over-segmentation results by using Otsu's algorithm. In order to extract precise cells in an image, the proposed

method comprised a simple classification procedure for IIF images to avoid over-segmentation.

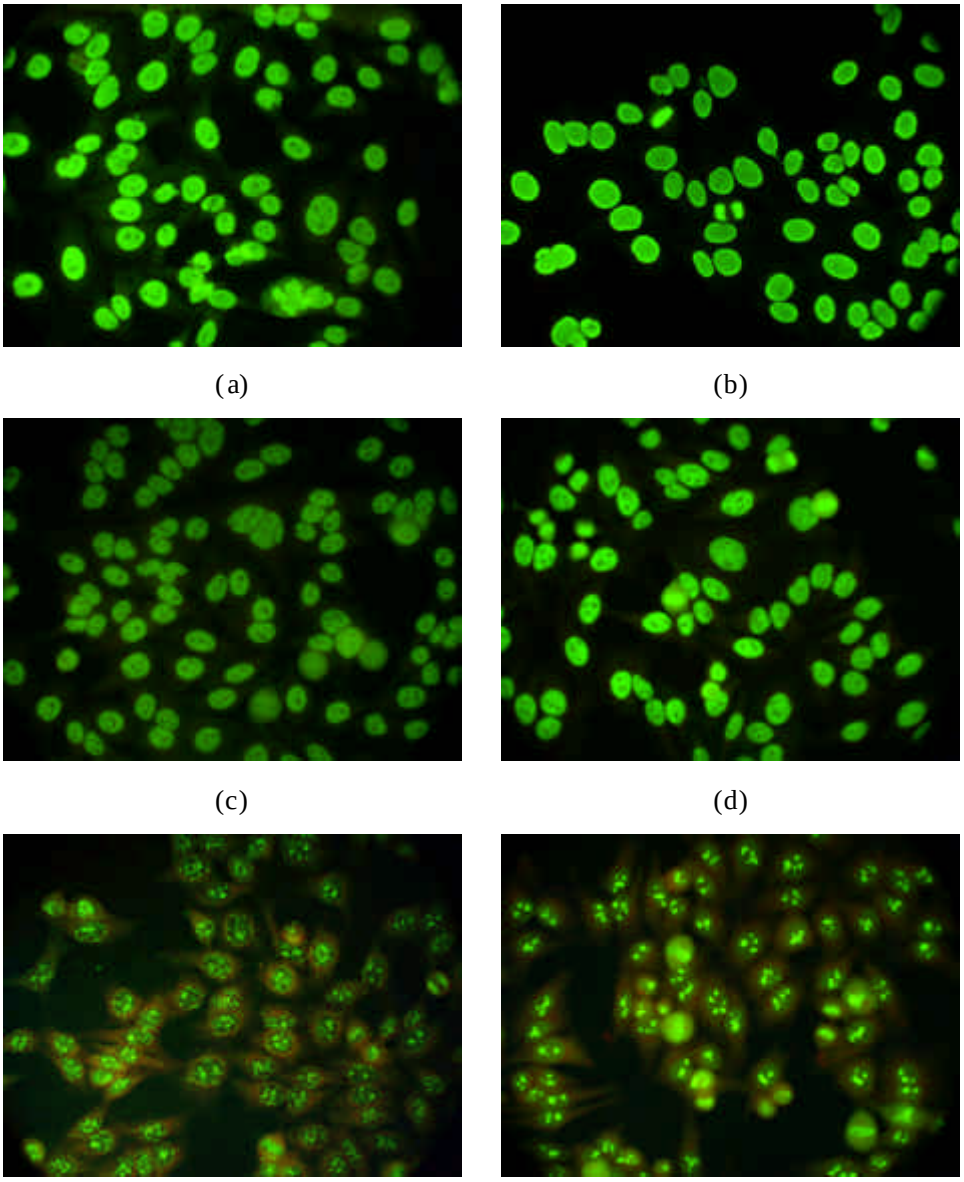

(a) (b)

(c) (d)

(e) (f)

Fig. 1. The six distinct autoantibody fluorescence patterns: (a) diffuse, (b) peripheral, (c) coarse speckled, (d) fine speckled, (e) discrete speckled, and (f) nucleolar.

Firstly, the automatic thresholding algorithm was performed to convert an IIF image to binary version. Then the proposed method counted the number of connected region in the binary image. The information of the connected region was used as the input of the IIF image classifier. We classified an IIF image into two cases based on the number of connected region n in an image:

Type 0 (image with sparse region cells): if the number of connected region n $\leq$ *T*;

Type 1 (image with mass region cells): if the number of connected region n $>$ *T*,

where *T* was the predefined threshold for identifying an IIF image with sparse region cells or with mass region cells. Based on the simple classification, the proposed method adaptive selected from two modules with different parameters to segment autoantibody fluorescence cells. Figure 3 presents a flowchart of the proposed method, in a form that includes the preprocessing and segmentation phases.

2.4 COLOR SPACES

A color space specifies how color information is represented; a color space is a model for representing color in terms of intensity values. Color space conversion is the translation of the representation of a color from one basis to another. This typically occurs in the context of converting an image that is represented in one color

space to another color space, the goal being to make the translated image look as similar as possible to the original. Sometimes, when we observe each channel in RGB color space, the information of IIF images can not be got, namely, the expected results of segmentation can not be acquired in this color space. Maybe transformation of color space is another ways to improve the segmentation results. In the view point of the proposed method, the Type 0 images were first converted to HSB (Hue, Saturation and Brightness channels) color space. We utilized the brightness (gray level) component as input image to segment cells.

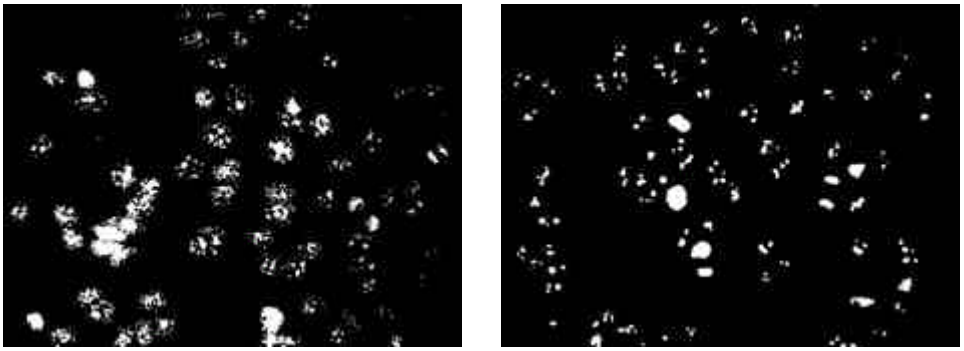

(a) (b)

Fig. 2. Over-segmentation in use of the Otsu's algorithm: (a) segmented result of Fig.1(e); (b) segmented result of Fig.1(f).

格式化: 內文, 靠左, 第一行: 0 字元

For Type 1 images, the original RGB image was transformed to CMY (Cyan, Magenta, and Yellow channels) color space. We found that the intensity dissimilarity between fluorescence cells and background was massive in the cyan component. Thus the cyan component was employed as input image to segment cells. In this study, the

HSI (hue, saturation, intensity) [16] and CMY (cyan, magenta, yellow) [17] color models were better than the RGB color space to segment IIF images.

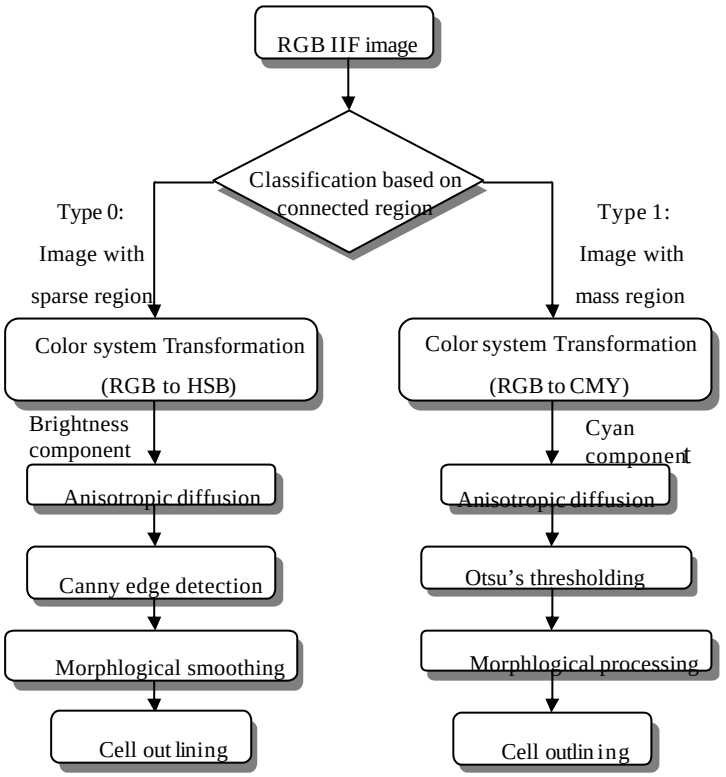

Fig. 3. The flowchart of the proposed adaptive segmentation method.

2.5 PREPROCESSING OF ANISOTROPIC DIFFUSION

Preprocessing is a significant issue before the segmentation. The effective preprocessing method for segmentation should aim to reduce noises and preserve the useful information, such as edge and boundary of the desired objects. The anisotropic diffusion method that based on a partial differential equation [18,19] is very practical

格式化: 字型色彩: 自動
格式化: 內文, 靠左, 縮排: 左: 0 cm, 凸出: 6 字元, 第一行: 0 字元
格式化: 行距: 固定行高 12 pt
格式化: 行距: 固定行高 12 pt
格式化: 行距: 固定行高 12 pt
刪除:
2.4 COLOR SPACES
A color space specifies how color information is represented; a color space is a model for representing color in terms of intensity values. Color space conversion is the translation of the representation of a color from one basis to another. This typically occurs in the context of converting an image that is represented in one color space to another color space, the goal being to make the translated image look as similar as possible to the original. Sometimes, when we observe each channel in RGB color space, the information of IIF images can not be got, namely, the expected results of segmentation can not be acquired in this color space. Maybe transformation of color space is another ways to improve the segmentation results. In the view point of the proposed method, the Type 0 images were first converted to HSB (Hue, Saturation and Brightness channels) color...

not only in image de-noising but also in preserving the important boundary information. The advantages of anisotropic diffusion include intra-region smoothing and edge preservation. Anisotropic diffusion performs well for images corrupted by additive noise. This study performed the anisotropic diffusion filter to enhance the IIF images for HEp-2 cell outlining. Figures 4 show the de-nosed results by applying the preprocessing method and two practical filters, i.e. the arithmetic average filter and Gaussian low-pass filter. Figure 1(a) is an original magnified monochrome IIF image that includes HEp-2 cells with various contrast levels and noises. The processed images obtained by arithmetic average filtering, Gaussian low-pass filtering and the anisotropic diffusion filtering are shown in Figs. 1(b)-(d), respectively. Obviously, the anisotropic diffusion method is superior to that two in removing noise and preserving edges for the IIF image. The proposed method using the preprocessing not only reduced the number of speckles and the amount of noises in images but also preserved the shape and contrast of fluorescence patterns.

2.6 ADAPTIVE IMAGE SEGMENTATION

For image with sparse region cells, the original RGB image was first transformed to HSI color model. The proposed method utilized the brightness (gray level) component as input image to segment cells. The anisotropic diffusion filter was

performed to enhance cell regions from background. Edge-based segmentation methods depend on the gradient of an image to determine objects' boundary. Such methods were designed to detect discontinuities of image intensity, so edge-based methods perform well when applied to Type 0 IIF images. This study employed a practical method, i.e. the Canny edge detector[20], to identify the edge information in an image and enhanced the detected edges by using the morphological dilation operator[21].

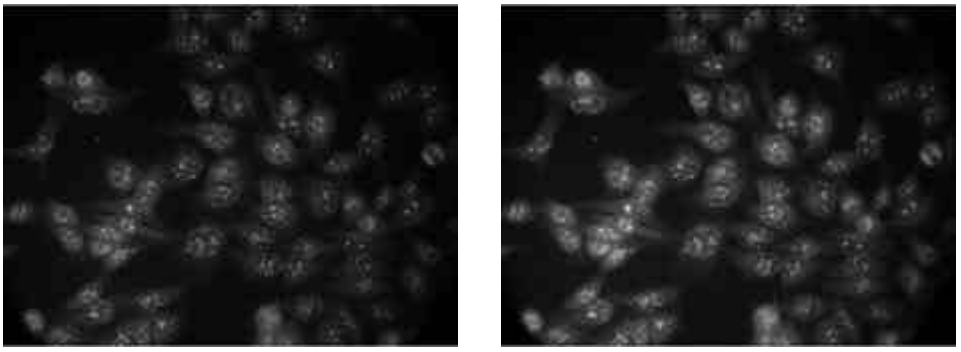

(a) (b)

Fig. 4. Example of the de-nosed results by applying the arithmetic average filter and Gaussian low-pass filter: (a) transformed gray image from original RGB image, (b) after arithmetic average filter and Gaussian low-pass filter.

Canny operator is one of the most excellent edge detection method. It can get single pixel width edge, and moreover, it includes Gaussian convolution which can suppresses the noise in the luminance difference. Canny optimizes edge response with respect to three criteria: a) Detection: real edges should not be missed, and false edges

should be avoided; b) Location: the edge response should lie as close as possible to its true location; c) One response: a true edge should not give rise to more than one response. Hence this study chosen Canny operator to detect edge. Finally, the morphological operator erosion and dilation were alternately utilized to fill the gaps within a cell and smooth outline of the segmented cell. Figures 5 demonstrate the processing results by this module in the proposed method.

Furthermore, for image with mass region cells, the original RGB image was transformed to CMY color space using Equations (2). We found that the intensity dissimilarity between fluorescence cells and background was massive in the cyan component. Thus the proposed method utilized the cyan component as input image to segment cells in the image with mass region cells. The anisotropic diffusion filter was also performed to enhance cell regions from background. The binary image with cell region segmentation could be generated by using the Otsu algorithm.

Otsu algorithm is well known and widely used, and is highly ranked in a comparative study of global binarization methods. It is suitable for real-time image processing due to its simplicity and high speed. But there is still one limitation of Otsu's method is that it does not work well with variable illumination. So the global threshold determined by Otsu's method is significant. In this module, the morphological operator opening and closing with a larger sized structuring element

刪除: so

were performed to diminish the region with a unreasonable size and then obtained the precise outline of the cells. Figures 6 show the processing results by segmentation module for Type 1 images.

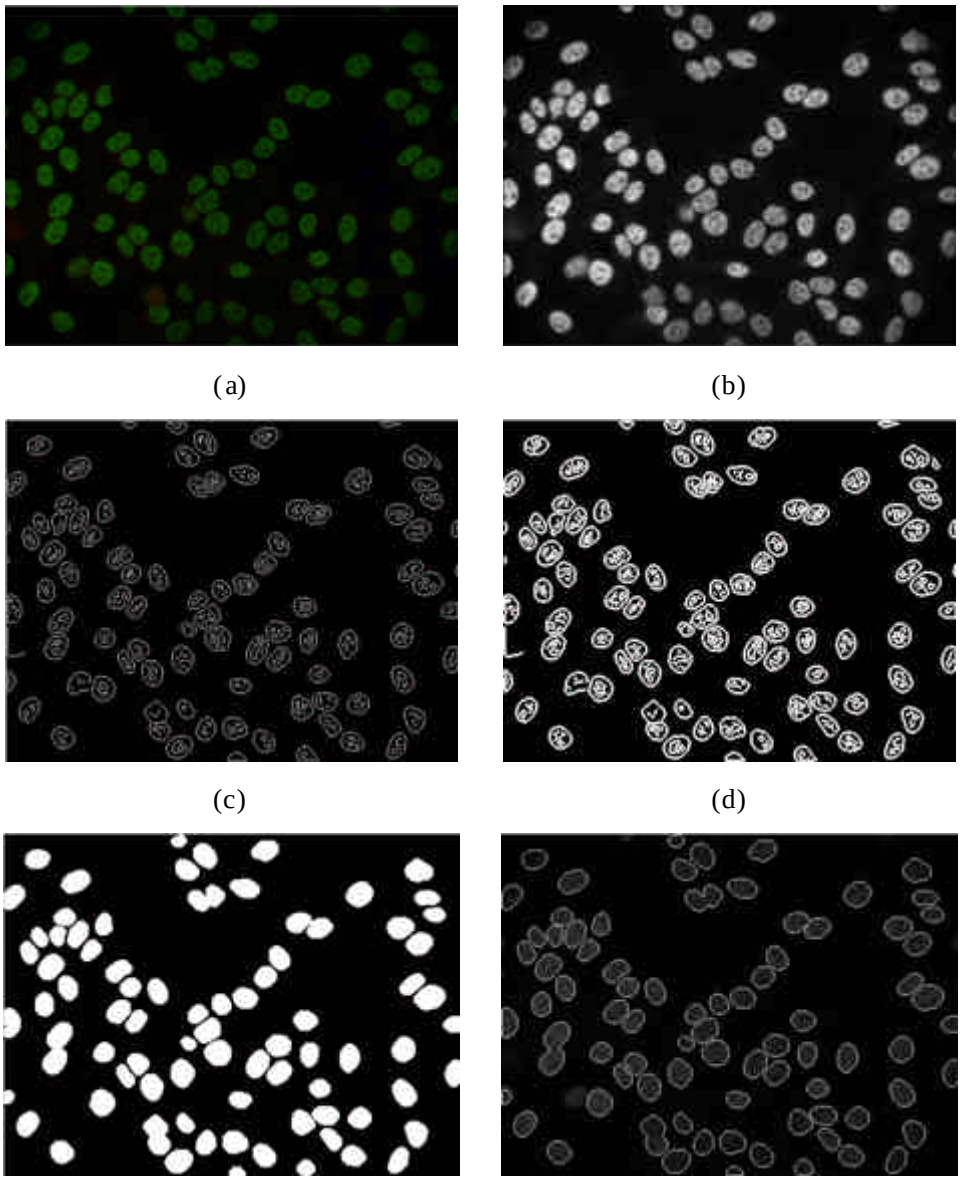

Fig. 5. An IIF image (with coarse speckled patterns) processed with the Type 0 segmentation module: (a) original RGB image, (b) transformed brightness image after the anisotropic diffusion filtering, (c) after Canny edge detection, (d) after morphological dilation, (e) after morphological smoothing, and (f) the outline of the segmented cell.

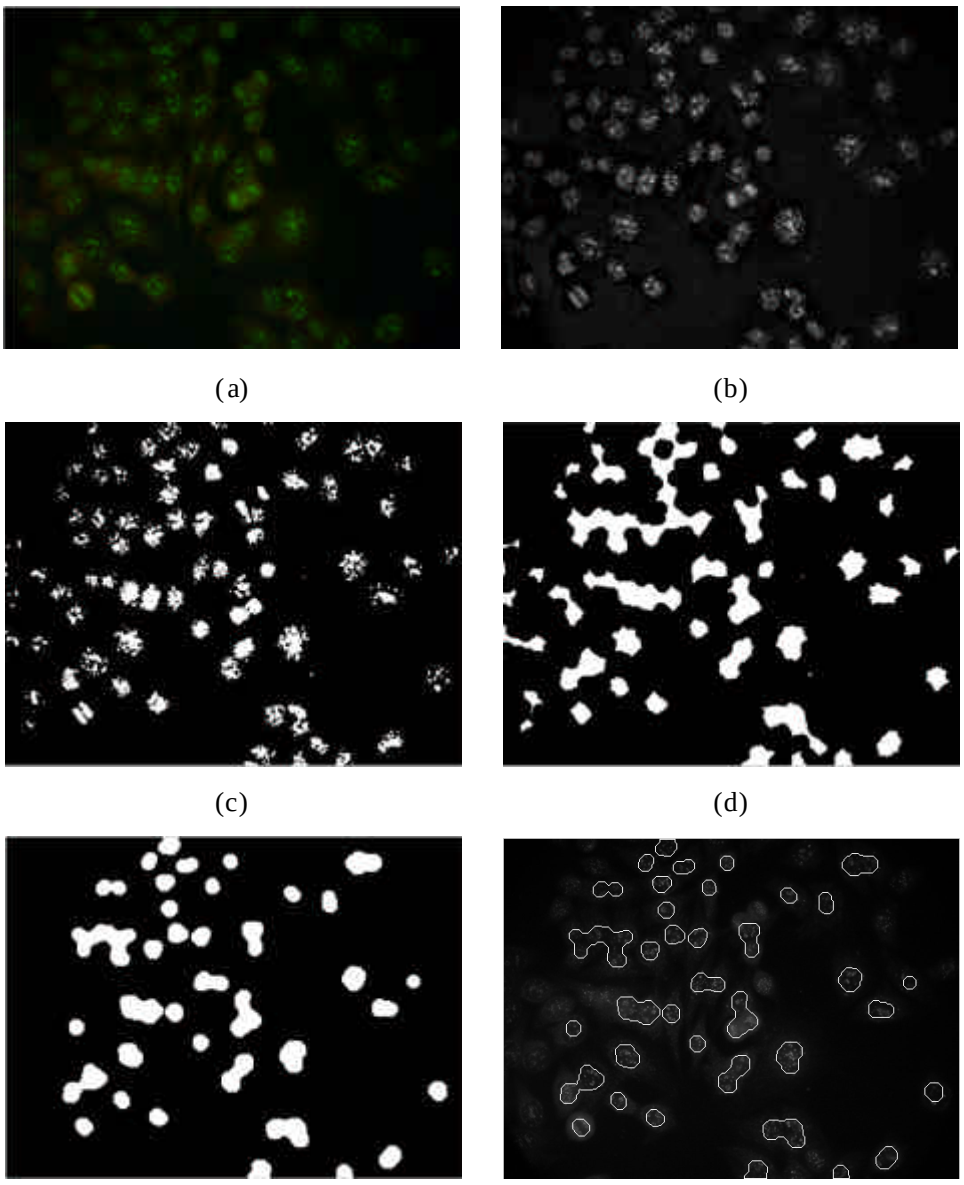

Fig. 6. An IIF image (with discrete speckled patterns) processed with the Type 1 segmentation module: (a) original RGB image, (b) transformed cyan image after the anisotropic diffusion filtering, (c) after automatic thresholding, (d) after morphological closing, (e) after morphological opening, and (f) the outline of the segmented cell.

CHAPTER 3

TEXTURE FEATURES ANALYSIS

Texture is one of the main features intensively utilized in image processing and pattern recognition. Texture feature of image is the spatial information about pixels' structural arrangement and their relationship with the surrounding environment. If pixels of an image are constant, we can say that the image has no texture. If pixels vary unevenly in values, then the image has many textures. Many approaches were developed to extract the texture features of an image. In this study, the textural features include block difference of inverse probabilities (BDIP) [22], block variation of local correlation coefficients (BVLC) [22], auto-covariance matrix [23,24], spatial gray-level dependence matrices (SGLDM) [25,26], and gray-level difference matrix (GLDM) [25,26]. The textural features were presented as follows in detail.

刪除: value

3.1 BLOCK DIFFERENCE OF INVERSE PROBABILITIES (BDIP)

The block difference of inverse probabilities (BDIP), which is one of the proposed texture features, is a block-based version of the difference of inverse probabilities. It is defined as the difference between the number of pixels in a block and the ratio of the sum of pixel intensities in the block to the maximum in the block.

$$BDIP = M^2 - \frac{\sum_{(i,j)\in B} I(i,j)}{\max_{(i,j)\in B} I(i,j)}, \qquad (1)$$

where $I(i,j)$ denotes the intensity of a pixel (i,j) and B is a block of size $M \times M$. The larger the variation of intensities there is in a block, the higher the value of BDIP. In this paper, the block size is chosen as 2×2 and higher BDIP values are shown darker.

3.2 BLOCK VARIATION OF LOCAL CORRELATION COEFFICIENTS (BVLC)

The variation of local correlation coefficients is known to measure texture smoothness well. It is defined as the variation, or the difference between the maximum and minimum, of local correlation coefficients according to four orientations. The block variation of local correlation coefficients (BVLC), is a block-based version of the variation of local correlation coefficients. Each local correlation coefficient is defined as local covariance normalized by local variance.

$$r(k,l) = \frac{\frac{1}{M^2}\sum_{(i,j)\in B} I(i,j)I(i+k,j+l) - m_{0,0}m_{k,l}}{s_{0,0}s_{k,l}}, \qquad (2)$$

where B denotes a block of size $M \times M$, $m_{0,0}$ and $s_{0,0}$ denote the local mean and standard deviation of the block B, respectively. The notation (k,l) denotes a

pair of horizontal shift and vertical shift associated with the four orientations $(-90^\circ, 0^\circ, -45^\circ, 45^\circ)$. As a result, $m_{k,l}$ and $s_{k,l}$ represent the mean and standard deviation of the block shifted by (k,l), respectively. The value of BVLC is defined as follows:

删除:

$$BVLC = \max_{(k,l)\in O_4}[r(k,l)] - \min_{(k,l)\in O_4}[r(k,l)], \quad (3)$$

$$O_4 = \{(0,1),(1,0),(1,1),(1,-1)\}. \quad (4)$$

From the above equation, we see that the larger the degree of roughness there is in a block, the higher the value of BVLC.

3.3 2-D NORMALIZED AUTO-COVARIANCE COEFFICIENTS

Different patterns in the IIF images have significantly different textures. The 2-D normalized auto-correlation coefficients used to reflect the inter-pixel correlation within an image. The coefficients are further modified into a mean-removed version to generate the similar auto-covariance features for images with different brightness but with a similar texture. This thesis used the correlation between neighboring pixels within the images as features. The modified auto-covariance coefficients between pixel (i, j) and pixel $(i+\Delta m, j+\Delta n)$ in an image with size $M \times N$ were defined as:

$$g(\Delta m, \Delta n) = \frac{A(\Delta m, \Delta n)}{A(0,0)} \quad (5)$$

where

$$A(\Delta m, \Delta n) = \frac{1}{(M-\Delta m)(N-\Delta n)} \sum_{x=0}^{M-1-\Delta m} \sum_{y=0}^{N-1-\Delta n} \left| \left(f(x,y) - \overline{f} \right) \left(f(x+\Delta m, y+\Delta n) - \overline{f} \right) \right| \quad (6)$$

where $\overline{f}$ is the mean value of $f(x,y)$. The dimension of the auto-covariance matrix can be any size of images. There will form an auto-covariance matrix which size is $\Delta m \times \Delta n$. In this study, Δm and Δn are both 5, after the processing of texture analysis, a $\Delta m \times \Delta n$ auto-covariance matrix is obtained for each image. Because the value of $g(0,0)$ is always one. The first element in matrix of every pattern will be discarded.

3.4 SPATIAL GRAY-LEVEL DEPENDENCE MATRICES (SGLDM)

The spatial gray-level dependence matrices (SGLDM) are introduced as a texture measure that accounts for the spatial variation and spatial dependence among the gray levels in the texture. The SGLDM are based on the estimation of the second-order joint conditional probability density functions, $f(i,j;d,q)$. Each $f(i,j;d,q)$ is the probability of going from gray-level i to j, given that the intersample spacing is d and the direction is specified by the angle q. The possible angle values are a multiple of 45 degrees. A total of 13 features can be extracted from the probability

function $f(i, j; d, q)$. Based on this, the following texture measures were computed:

格式化: 靠左, 縮排: 左 1 字元

1. Angular second moment
2. Contrast
3. Correlation
4. Sum of squares: variance
5. Inverse difference moment
6. Sum average
7. Sum variance
8. Sum entropy
9. Entropy
10. Difference variance
11. Difference entropy
12. and 13. Information measures of correlation

This study utilizes one of the 13 possible useful features, i.e. entropy E.

$$E = -\sum_i \sum_j q(i, j \mid d) \log S_q(i, j \mid d), \qquad (7)$$

格式化: 置中

where $S_q(i, j \mid d)$ is the $(i, j)^{th}$ element of S_q when distance = d. In this thesis, the distance is 1 and for angles $q = 0^\circ$, 45°, 90° and 135° and then we computed four values for entropy texture measure.

3.5 GRAY-LEVEL DIFFERENCE MATRIX (GLDM)

A gray-level difference matrix is based on the occurrence of two pixels that have a given absolute difference in gray level and that are separated by a specific

displacement. Digital gray-scaled images can be represented as a function of intensity and coordinate $I(x,y)$. Let $I_s(x,y) = |I(x,y) - I(x+\Delta x, y+\Delta y)|$ for any given displacement $s = (\Delta x, \Delta y)$ and $f'(i|s)$ is the probability function of $I_s(x,y)$. In the current study, four possible forms for $s = (\Delta x, \Delta y)$ are considered, $(0,d)$, $(-d,d)$, $(d,0)$, and $(-d,-d)$, where d is the displacement between pixel x and y. Only one feature is used in this thesis, i.e. inverse difference moment (IDM). The definition of this feature is given as:

删除: intersample spacing distance

$$IDM = \frac{\sum_i f'(i|s)}{(i^2+1)}, \qquad (8)$$

格式化: 置中

where $i \in (0, N_G - 1)$ and N_G is the Maximum gray level value just like in SGLDM.

CHAPTER 4

EXPERIMENTS AND RESULTS

This study totally experimented 2573 autoantibody fluorescence patterns with manual sketched outlines (including 519 diffuse patterns, 482 peripheral patterns, 788 coarse speckled patterns, 634 fine speckled patterns, 64 discrete speckled patterns and 86 nucleolar patterns) from 45 IIF images to test the accuracy of the proposed method. These simulations were made on a single CPU Intel Pentium-VI 3.0 GHz personal computer with Microsoft Windows XP operating system.

In this work, the Otsu's algorithm was first performed to calculate the number of connected region that used as the input of the IIF image classifier. With the predefined threshold T ranged from 200 to 400, the proposed adaptive segmentation system obtained a stable and the highest accuracy. Moreover, the morphological dilation operators for image with sparse region cells (Type 0) utilized a 3 × 3 diamond-shaped structuring element. The morphological dilation operators for image with mass region cells (Type 1) employed a 17 × 17 diamond-shaped structuring element.

格式化: 字型: 斜體

刪除:

Table 1 lists the segmentation results that made a comparison between the proposed method and the Otsu automatic thresholding with morphological operators. The number of the segmented divided and mixed cells might be used to evaluate the

accuracy of the segmentation results. However, there are various cases are mixed indeed. In these cases, serious overlapping could be found between the cells. Besides this circumstance, the proposed system clearly yielded cell outlines that are similarly to those manually sketched. From the segmentation results, only a small number of cases might generate an undesired segmentation.

Table 1. Comparisons for fluorescence patterns segmentation between the proposed method and the Otsu's automatic thresholding with morphological operators.

Autoantibody fluorescence pattern		The Otsu algorithm with morphlogical processing		The proposed method	
	no. manual sketched cells	no. divided cells	no. mixed cells	no. divided cells	no. mixed cells
Diffuse	519	169	90	394	50
Peripheral	482	180	80	326	63
Coarse speckled	788	232	135	636	52
Discrete speckled	634	239	72	431	48
Fine speckled	64	11	14	50	4
Nucleolar	86	41	17	72	4

Although several classification methods exist such as neural networks, k-nearest neighbor and logistic regression, we still choose to employ the binary decision tree induction algorithm. Because the decision tree induction process does not only act as

a knowledge discovery process, but also works as a feature selector, discovering a subset from the whole set of features in the sample set that is the most relevant to the problem solution. This algorithm learns a set of rules and basic features necessary for decision making. It partitions the decision space recursively into sub-regions based on the sample set. In this way, the decision tree recursively breaks down the complexity of the decision space.

删除: it

删除: o f features

删除: allows one to

In operations research, specifically in decision analysis, a decision tree is a decision support tool that uses a graph or model of decisions and their possible consequences, including chance event outcomes, resource costs, and utility. A decision tree is used to identify the strategy most likely to reach a goal. Another use of trees is as a descriptive means for calculating conditional probabilities.

Figure 7 shows the structure of a binary decision tree. A binary decision tree consists of nodes and branches. Each node represents a single test or decision. In the case of a binary tree, the decision is either true or false. The starting node is usually referred to as the root node. Depending on whether the result of a test is true or false, the tree will branch right or left to another node. Finally, a terminal node is reached, and a decision is made on the class assignment.

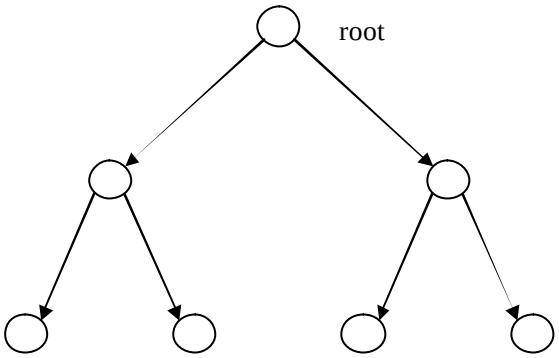

Fig. 7. The structure of a binary decision tree.

In the proposed classification, a dataset with 600 fluorescence patterns was utilized to simulation. The dataset contained six classes, and for each class were equally distributed and included 100 patterns. Then the k-fold cross validation method was used to evaluate the accuracy and performance of the classifiers trained using textural features. The k-fold cross validation method can be summarized as follows: a) The training samples are arbitrarily divided into *k* subsets. b) One of the subsets is left out for evaluation and the parameters of the classifier are learned using the samples in the remaining *k*-1 subsets. The recognition rate corresponding to the subset left for evaluation is calculated using the trained classifier. Since there are *k* possibilities for how to leave out the subset for evaluation, the recognition rates of all *k* subsets are evaluated. c) The final generalization performance is computed as the average of the recognition rate for the *k* subsets.

刪除: our
刪除: we used a
刪除: o f
刪除: images
刪除: each
刪除: equally distributed
刪除: . F
刪除: we had
刪除: images
刪除: Afterward, we
刪除:
刪除: used
格式化: 字型: 斜體
格式化: 字型: 斜體
刪除:
格式化: 字型: 斜體

Table 2 reveals the classification results that made a comparison between the accuracy and performance with all kinds of *k* values and levels of the binary decision tree. It can be seen from the table, no matter what the *k* value is, the accuracy still makes no difference under the same levels of the binary decision tree. Even though the accuracy be improved via increased the levels, the performance has also became more and more worse. How to keep balance between the accuracy and performance are the most significant issue for us.

Table 2. Comparisons for fluorescence patterns classification between the accuracy and performance with all kinds of k values and levels of the binary decision tree.

k values	*k* = 2		*k* = 5		*k* = 10	
	Accuracy	Performance	Accuracy	Performance	Accuracy	Performance
5 levels	79.33%	6.5s	79.34%	7s	79.33%	7s
10 levels	83.67%	11.5s	83.67%	12s	83.67%	13.9s

CHAPTER 5

CONCLUSION

This thesis presented an efficient method for automatically detecting outlines of fluorescence cells in IIF images. The preprocessing of the proposed method applied an anisotropic diffusion filter to reduce the any amount of noises but preserved the shape and contrast of fluorescence cell. This study classified an IIF image into two cases based on the number of connected region in an image. The proposed adaptive segmentation method was used to generate precise outline of the cells based on the types of image. The IIF image database including 2573 cases were used to evaluation. We found that the proposed method determines the outlines of fluorescence cells that are very similar to manual sketched ones. Segmentation results revealed that the proposed method can practically segment fluorescence cells from IIF images.

In the future, the proposed method can focused on the segmentation improvement. Due to the technique of data acquisition is not skillful, the large number of overlapped cell, the tiny variation between fluorescence cells and background, and the autoantibody fluorescence pattern is very difficult to segment. As long as these problems can be overcame step by step, the accuracy of the proposed automatic segmentation will increase than before. By this way, an assisting segmentation system could notably facilitate autoantibody diagnostics.

刪除: article

刪除: We need to

刪除: improve

刪除: results first in the future

刪除: and

In the classification, the experiment based on the objective feature measurements gave us new insights into the application. The performance of the resulting classifier isn't worse than the performance of the expert. The classifier can decide based on the image features of a single cell, while the expert needs mitosis to make a final decision. Further developing the texture feature will do further improvement of the classification procedure.

REFERENCES

[1] H.S.Wu and J.Barba, "An efficient semi-automatic algorithm for cell contour extraction," *J. Microscopy*, vol. 179 pp. 270-276, Sept. 1995.

[2] H.S.Wu, J.Barba, and J.Gil, "Iterative thresholding for segmentation of cells from noisy images," *J. Microscopy*, vol. 197 pp. 296-304, 2000.

[3] H.S.Wu and J.Gil, "An iterative algorithm for cell segmentation using short-time Fourie r transform," *J. Microscopy*, vol. 184 pp. 127-132, 1996.

[4] H.S.Wu, J.Barba, and J.Gil, "A parametic fitting algorithm for segmentation of cell images," *IEEE Trans. Biomed. Eng.*, vol. 45 pp. 400-407, 1998.

[5] T.Mouroutis, S.J.Roberts, and A.A.Bharath, "Robust cell nuclei segmentation using statistical modeling," *Bioimaging*, vol. 6 pp. 79-91, 1998.

[6] A.Garrido and N.Perez, "Applying deformable templates for cell image segmentation," *Pattern Recognit*, vol. 33 pp. 821-832, 2000.

[7] I.Simon, C.R.Pound, A.W.Partin, J.Q.Clemens, and W.A.Christensbarry, "Automated image analysis system for detecting boundaries of live prostate cancer cells," *Cytometry*, vol. 31 pp. 287-294, 1998.

[8] H.S.Wu and J.Barba, "An algorithm for noisy cell contour extraction via area merging," *J. Imag. Sci. , Technol.*, vol. 38 pp. 604-607, 1994.

[9] R.Adams and L.Bischof, "Seeded region growing," *IEEE Trans. Pattern Analys. Machine Intell.*, vol. 16 pp. 641-647, June 1994.

[10] M.A.Wani and B.G.Batchelor, "Edge-region-based segmentation of range images," *IEEE Trans. Pattern Analys. Machine Intell.*, vol. 16 pp. 314-319, Mar. 1994.

[11] J.Canny, "Computational approach to edge detection," *IEEE Trans. Pattern Anal. Machine Intell.*, vol. PAMI-8 pp. 679-698, 1986.

[12] Y.H.Kim and S.D.Kim, "Image flow segmentation and estimation using displaced spatial gradient," *Inst. Electr. Eng. Electronics Lett.*, vol. 28 pp. 2213-2215, 1992.

[13] S.Sarkar and K.Boyer, "On optimal infinite impulse response edge detection filters," *IEEE Trans. Pattern Analys. Machine Intell.*, vol. 13 pp. 1154-1171, Nov. 1991.

[14] W.N.Lie, "Automatic target segmentation by locally adaptive image thresholding," *IEEE Trans. Image Process.*, vol. 4 pp. 1036-1041, July 1995.

[15] Otsu N, "Threshold Selection Method from Gray-Level Histograms," *IEEE Transactions on Systems Man and Cybernetics*, vol. 9 pp. 62-66, 1979.

[16] Chungcheng LEE and Chulung CHEN, "A Mach-Zehnder joint transform correlator using encoding technique with reflective spatial light modulators based on the HSV color space," 2006.

[17] Marko TkalEiE and Jurij F.TasiE, "Colour spaces - perceptual, historical and applicational background," 2003.

[18] P.Perona and J.Malik, "Scale-space and edge detection using anisotropic diffusion," *IEEE Trans. Pattern Analys. Machine Intell.*, vol. 12 pp. 629-639, 1990.

[19] M.J.Black, G.Sapiro, D.H.Marimont, and D.Heeger, "Robust anisotropic diffusion," *IEEE Trans. Image Process.*, vol. 7 pp. 421-432, 1998.

[20] Canny J, "A Computational Approach to Edge Detection," *IEEE Trans. Pattern Anal. Machine Intell.*, vol. PAMI-8 pp. 679-698, 1986.

[21] Gonzalez RC and Woods RE, *Digital image processing. 2 ed.* 2002.

[22] D.C.Young, Y.S.Sang, and C.K.Nam, "Image retrieval using BDIP and BVLC moments," *IEEE Transactions on Circuits and Systems for Video Technology*, vol. 13 pp. 951-957, 2003.

[23] W.M.Chen, R.F.Chang, S.J.Kuo, C.S.Chang, W.K.Moon, and S.T.Chen, "3-D

ultrasound texture classification using run difference matrix," *Ultrasound Med. Biol*., vol. 31 pp. 763-770, June 2005.

[24] W.M.Chen, R.F.Chang, W.K.Moon, and D.R.Chen, "Breast cancer diagnosis using three-dimensional ultrasound and pixel relation analysis," *Ultrasound Med. Biol.*, vol. 29 pp. 1027-1035, July 2003.

[25] M.Amadasun and R.King, "Textural features corresponding to textural properties," *IEEE Transactions on Systems, Man and Cybernetics*, vol. 19 pp. 1264-1274, 1989.

[26] C.I.Christodoulou, C.S.Pattichis, M.Pantziaris, and A.Nicolaides, "Texture-based classification of atherosclerotic carotid plaques," *IEEE Transactions on Medical Imaging*, vol. 22 pp. 902-912, 2003.

2.4 COLOR SPACES

A color space specifies how color information is represented; a color space is a model for representing color in terms of intensity values. Color space conversion is the translation of the representation of a color from one basis to another. This typically occurs in the context of converting an image that is represented in one color space to another color space, the goal being to make the translated image look as similar as possible to the original. Sometimes, when we observe each channel in RGB color space, the information of IIF images can not be got, namely, the expected results of segmentation can not be acquired in this color space. Maybe transformation of color space is another ways to improve the segmentation results. In the view point of the proposed method, the Type 0 images were first converted to HSB (Hue, Saturation and Brightness channels) color space. We utilized the brightness (gray level) component as input image to segment cells. For Type 1 images, the original RGB image was transformed to CMY (Cyan, Magenta, and Yellow channels) color space. We found that the intensity dissimilarity between fluorescence cells and background was massive in the cyan component. Thus the cyan component was employed as input image to segment cells. In this study, the HSI (hue, saturation, intensity) [16] and CMY (cyan, magenta, yellow) [17] color models were better than the RGB color

space to segment IIF images.